Extrapolation in Time in Thermal Fluid Structure Interaction

Philipp Birken, Tobias Gleim, Detlef Kuhl and Andreas Meister

Abstract We consider time dependent thermal fluid structure interaction. The respective models are the compressible Navier-Stokes equations and the nonlinear heat equation. A partitioned coupling approach via a Dirichlet-Neumann method and a fixed point iteration is employed. As a reference solver a previously developed efficient time adaptive higher order time integration scheme is used. To improve upon this, we work on reducing the number of fixed point coupling iterations. Thus, we explore the idea of extrapolation based on data given from the time integration and derive such methods for SDIRK2. This allows to reduce the number of fixed point iterations further by up to a factor of two with linear extrapolation performing better than quadratic.

1 Introduction

Thermal interaction between fluids and structures plays an important role in many applications. Examples for this are cooling of gas-turbine blades, thermal anti-icing systems of airplanes [7] or supersonic reentry of vehicles from space [17, 13]. Another is quenching, an industrial heat treatment of metal workpieces. There, the desired material properties are achieved by rapid local cooling, which causes solid phase changes, allowing to create graded materials with precisely defined properties. Gas quenching recently received a lot of industrial and scientific interest [25, 12]. In contrast to liquid quenching, this process has the advantage of minimal environmental impact because of non-toxic quenching media and clean products like air [22]. To exploit the multiple advantages of gas quenching the application of computational

Philipp Birken, Centre for the Mathematical Sciences, Numerical Analysis, Lunds University, Box 118, 22100 Lund, Sweden, e-mail: philipp.birken@na.lu.se · Tobias Gleim and Detlef Kuhl, Institute of Mechanics and Dynamics, University of Kassel, Mönchebergstr. 7, 34109 Kassel, Germany, e-mail: tgleim,kuhl@uni-kassel.de · Andreas Meister, Institute of Mathematics, University of Kassel, Heinrich-Plett-Str. 40, 34132 Kassel, Germany, e-mail: meister@mathematik.uni-kassel.de

fluid dynamics has proved essential [2, 22, 16]. Thus, we consider the coupling of the compressible Navier-Stokes equations as a model for air, along a non-moving boundary with the nonlinear heat equation as a model for the temperature distribution in steel.

For the solution of the coupled problem, we prefer a partitioned approach [9], where different codes for the sub-problems are reused and the coupling is done by a master program which calls interface functions of the other codes. This allows to use existing software for each sub-problem, in contrast to a monolithic approach, where a new code is tailored for the coupled equations. To satisfy the boundary conditions at the interface, the subsolvers are iterated in a fixed point procedure. Our goal here is to find a fast solver in this partitioned setting. One approach would be to speed up the subsolvers and there is active research on that. See [4] for the current situation for fluid solvers. However, we want to approach the problem from the point of view of a partitioned coupling method, meaning that we use the subsolvers as they are. As a reference solver, we use the time adaptive higher order time integration method suggested in [6]. Namely, the singly diagonally implicit Runge-Kutta (SDIRK) method SDIRK2 is employed.

To improve upon this, one idea is to define the tolerances in the subsolver in a smart way and recently, progress has been made for steady problems [3]. However, it is not immediately clear how to transfer these results to the unsteady case. Thus, the most promising way is to reduce the number of fixed point iterations, on which we will focus in the present article. Various methods have been proposed to increase the convergence speed of the fixed point iteration by decreasing the interface error between subsequent steps, for example Relaxation [15, 14], Interface-GMRES [18], ROM-coupling [24] and multigrid coupling [23]. Here we follow instead the idea of extrapolation based on knowledge about the time integration scheme. This has been successfully used in other contexts [1, 8], but has to our knowledge never been tried in Fluid Structure Interaction, where typically little attention is given to the time integration. Here, we use linear and quadratic extrapolation of old values from the time history, designed specifically for SDIRK2. The various methods are compared on the basis of numerical examples, namely the flow past a flat plate, a basic test case for thermal fluid structure interaction, an example from gas quenching [25] and flow past a cylinder.

2 Governing Equations

The basic setting we are in is that on a domain $\Omega_1 \subset \mathbb{R}^d$ the physics is described by a fluid model, whereas on a domain $\Omega_2 \subset \mathbb{R}^d$, a different model describing the structure is used. The two domains are almost disjoint in that they are connected via an interface. The part of the interface where the fluid and the structure are supposed to interact is called the coupling interface $\Gamma \subset \partial\Omega_1 \cup \partial\Omega_2$. Note that Γ might be a true subset of the intersection, because the structure could be insulated. At the interface Γ, coupling conditions are prescribed that model the interaction between fluid and

structure. For the thermal coupling problem, these conditions are that temperature and the normal component of the heat flux are continuous across the interface.

2.1 Fluid Model

We model the fluid using the time dependent Reynolds Averaged Navier-Stokes (URANS) equations, which are a second order system of conservation laws (mass, momentum, energy) modeling turbulent compressible flow. We consider the two dimensional case, written in conservative variables density ρ, momentum $\mathbf{m} = \rho\mathbf{v}$ and energy per unit volume ρE, where a $\tilde{}$ denotes the Favre average and the overbar the ensemble average:

$$\begin{aligned}
&\partial_t \overline{\rho} + \nabla \cdot \overline{\rho}\tilde{\mathbf{v}} = 0, \\
&\partial_t \overline{\rho}\tilde{\mathbf{v}} + \sum_{j=1}^{2} \partial_{x_j}(\overline{\rho}\tilde{v}_i\tilde{v}_j) = -\partial_{x_j}\overline{p}\delta_{ij} + \frac{1}{Re}\sum_{j=1}^{2}\partial_{x_j}\left(\tilde{S}_{ij} + S_{ij}^R\right), \quad i = 1,2 \\
&\partial_t \overline{\rho}\tilde{E} + \nabla \cdot (\overline{\rho}\tilde{H}\tilde{v}_j) = \sum_{j=1}^{2}\partial_{x_j}\left(\overline{(\frac{1}{Re}S_{ij} - S_{ij}^R)v_i} - \overline{\rho}\widetilde{v_j''} + \widetilde{S_{ij}v_i^{ii}} - \overline{\rho}\widetilde{v_j''k} + \frac{\overline{W}_j}{RePr}\right).
\end{aligned} \tag{1}$$

The Reynolds stresses

$$S_{ij}^R = -\overline{\rho}\widetilde{v_i''v_j''}$$

and the turbulent energy

$$k = \frac{1}{2}\sum_{j=1}^{d}\overline{v_j'v_j'}$$

are modelled using the Spallart-Allmaras model [21]. Furthermore, $\mathbf{q} = (q_1, q_2)^T$ represents the heat flux and $\mathbf{S} = (S_{ij})_{i,j=1,2}$ the viscous shear stress tensor. As the equations are dimensionless, the Reynolds number Re and the Prandtl number Pr appear. The system is closed by the equation of state for the pressure $p = (\gamma - 1)\rho e$, the Sutherland law representing the correlation between temperature and viscosity as well as the Stokes hypothesis. Additionally, we prescribe appropriate boundary conditions at the boundary of Ω_1 except for Γ, where we have the coupling conditions. In the Dirichlet-Neumann coupling, a temperature value is enforced strongly at Γ.

2.2 Structure Model

Regarding the structure model, we will consider heat conduction only. Thus, we have the nonlinear heat equation for the structure temperature Θ

$$\rho(\mathbf{x})c_p(\Theta)\frac{d}{dt}\Theta(\mathbf{x},t) = -\nabla\cdot\mathbf{q}(\mathbf{x},t), \tag{2}$$

where

$$\mathbf{q}(\mathbf{x},t) = -\lambda(\Theta)\nabla\Theta(\mathbf{x},t)$$

denotes the heat flux vector. For steel, the specific heat capacity c_p and heat conductivity λ are temperature-dependent and highly nonlinear. Here, an empirical model for the steel 51CrV4 suggested in [20] is used. This model is characterized by the coefficient functions

$$\lambda(\Theta) = 40.1 + 0.05\Theta - 0.0001\Theta^2 + 4.9\cdot 10^{-8}\Theta^3 \tag{3}$$

and

$$c_p(\Theta) = -10\ln\left(\frac{e^{-c_{p1}(\Theta)/10} + e^{-c_{p2}(\Theta)/10}}{2}\right) \tag{4}$$

with

$$c_{p1}(\Theta) = 34.2e^{0.0026\Theta} + 421.15 \tag{5}$$

and

$$c_{p2}(\Theta) = 956.5e^{-0.012(\Theta-900)} + 0.45\Theta. \tag{6}$$

For the mass density one has $\rho = 7836\,\mathrm{kg/m^3}$. Finally, on the boundary, we have Neumann conditions $\mathbf{q}(\mathbf{x},t)\cdot\mathbf{n}(\mathbf{x}) = q_b(\mathbf{x},t)$.

3 Discretization

3.1 Discretization in space

Following the partitioned coupling approach, we discretize the two models separately in space. For the fluid, we use a finite volume method, leading to

$$\frac{d}{dt}\mathbf{u} + \mathbf{h}(\mathbf{u},\Theta) = \mathbf{0}, \tag{7}$$

where $\mathbf{h}(\mathbf{u},\Theta)$ represents the spatial discretization and its dependence on the temperatures in the fluid. In particular, the DLR TAU-Code is employed [10], which is a cell-vertex-type finite volume method with AUSMDV as flux function and a linear reconstruction to increase the order of accuracy. Regarding structural mechanics, the use of finite element methods is ubiquitous. Therefore, we will also follow that approach here and use quadratic finite elements [26], leading to the nonlinear equation for all unknowns on Ω_2

$$\mathbf{M}(\Theta)\frac{d}{dt}\Theta + \mathbf{K}(\Theta)\Theta = \mathbf{q}_b(\mathbf{u}). \tag{8}$$

Here, $\mathbf{M}$ is the heat capacity and $\mathbf{K}$ the heat conductivity matrix. The vector Θ consists of all discrete temperature unknowns and $\mathbf{q}_b$ is the heat flux vector on the surface. In this case it is the prescribed Neumann heat flux vector of the fluid.

3.2 Coupled time integration

For the time integration, a time adaptive SDIRK2 method is implemented in a partitioned way, as suggested in [6]. If the fluid and the solid solver are able to carry out time steps of implicit Euler type, the master program of the FSI procedure can be extended to SDIRK methods very easily, since the master program just has to call the backward Euler routines with specific time step sizes and starting vectors. This method is very efficient and will be used as the base method in its time adaptive variant, which is much more efficient than more commonly used fixed time step size schemes.

To obtain time adaptivity, embedded methods are used. Thereby, the local error is estimated by the solvers separately, which then report the estimates back to the master program. Based on this, the new time step is chosen [5]. To this end, all stage derivatives are stored by the subsolvers. If the possibility of rejected time steps is taken into account, the current solution pair $(\mathbf{u}, \Theta)$ has to be stored as well.

To comply with the conditions that the discrete temperature and heat flux are continuous at the interface Γ, a Dirichlet-Neumann coupling is used. Thus, the boundary conditions for the two solvers are chosen such that we prescribe Neumann data for one solver and Dirichlet data for the other. Following the analysis of Giles [11], temperature is prescribed for the equation with smaller heat conductivity, here the fluid, and heat flux is given on Γ for the structure. Choosing these conditions the other way around leads to an unstable scheme.

In the following it is assumed that at time t_n, the step size Δt_n is prescribed. Applying a DIRK method to equation (7)-(8) results in the coupled system of equations to be solved at Runge-Kutta stage i, $i = 1, 2$:

$$\mathbf{F}(\mathbf{u}_i, \Theta_i) := \mathbf{u}_i - \mathbf{s}_i^{\mathbf{u}} - \Delta t_n\, a_{ii}\mathbf{h}(\mathbf{u}_i, \Theta_i) = \mathbf{0}, \tag{9}$$

$$\mathbf{T}(\mathbf{u}_i, \Theta_i) := [\mathbf{M} + \Delta t_n\, a_{ii}\mathbf{K}]\Theta_i - \mathbf{M}\mathbf{s}_i^{\Theta} - \mathbf{q}_b(\mathbf{u}_i) = \mathbf{0}. \tag{10}$$

Here, $a_{ii} = 1 - \sqrt{2}/2$ is a coefficient of the time integration method and $\mathbf{s}_i^{\mathbf{u}}$ and $\mathbf{s}_i^{\Theta}$ are given vectors, called starting vectors, computed inside the DIRK scheme. The dependence of the fluid equations $\mathbf{h}(\mathbf{u}_i, \Theta_i)$ on the temperature Θ_i results from the nodal temperatures of the structure at the interface. This subset is written as Θ_i^{Γ}. Accordingly, the structure equations depend only on the heat flux of the fluid at the coupling interface.

4 Fixed Point Iteration and Improvements

4.1 Basic fixed point iteration

To solve the coupled system of nonlinear equations (9)-(10), a strong coupling approach is employed. Thus, a fixed point iteration is iterated until a convergence criterion is satisfied. In particular, we use a a nonlinear Gauß-Seidel process:

$$\mathbf{F}(\mathbf{u}_i^{(\nu+1)}, \Theta_i^{(\nu)}) = \mathbf{0} \quad \rightsquigarrow \quad \mathbf{u}_i^{(\nu+1)} \tag{11}$$

$$\mathbf{T}(\mathbf{u}_i^{(\nu+1)}, \Theta_i^{(\nu+1)}) = \mathbf{0} \quad \rightsquigarrow \quad \Theta_i^{(\nu+1)}, \quad \nu = 0, 1, ... \tag{12}$$

Each inner iteration is thereby done locally by the structure or the fluid solver. More specific, a Newton method is used in the structure and a FAS multigrid method is employed in the fluid. In the base method, the starting values of the iteration are given by $\mathbf{u}_i^{(0)} = \mathbf{s}_i^{\mathbf{u}}$ and $\Theta_i^{(0)} = \mathbf{s}_i^{\Theta}$. The termination criterion is formulated by the relative update of the nodal temperatures at the interface of the solid structure and the tolerance is chosen to avoid iteration errors to interfere with the error estimation in the time adaptive method. Thus we stop once we are below the tolerance in the time integration scheme divided by five

$$\|\Theta_i^{\Gamma\,(\nu+1)} - \Theta_i^{\Gamma\,(\nu)}\| \leq TOL/5 \|\Theta_i^{\Gamma\,(0)}\|. \tag{13}$$

The vector

$$\mathbf{r}^{(\nu+1)} := \Theta_i^{\Gamma\,(\nu+1)} - \Theta_i^{\Gamma\,(\nu)} \tag{14}$$

is often referred to as the interface residual. We will now consider different techniques to improve upon this base iteration, namely extrapolation inside the time integration schemes, to obtain better initial values and then using vector extrapolation inside the fixed point iteration to speed up the iteration.

4.2 Extrapolation from time integration

To find good starting values for iterative processes in implicit time integration schemes, it is common to use extrapolation based on knowledge about the trajectory of the solution of the initial value problem [8, 19]. In the spirit of partitioned solvers, we here suggest to use extrapolation of the interface temperatures only. On top, this strategy could be used as well within the subsolvers, but we will not consider this here and use those solvers as they are. We now derive extrapolation methods for SDIRK2.

At the first stage, we have the old time step size Δt_{n-1} with value Θ_{n-1} and the current time step size Δt_n with value Θ_n. We are looking for the value Θ_n^1 at the next stage time $t_n + c_1 \Delta t_n$ with $c_1 = a_{11}$. Linear extrapolation results in

$$\Theta_n^1 \approx \Theta_n + c_1\Delta t_n(\Theta_n - \Theta_{n-1})/\Delta t_{n-1} = \left(1 + \frac{c_1\Delta t_n}{\Delta t_{n-1}}\right)\Theta_n - \frac{c_1\Delta t_n}{\Delta t_{n-1}}\Theta_{n-1}. \quad (15)$$

An alternative would be the intermediate temperature vector Θ_{n-1}^1 from the previous stage $t_{n-1} + c_1\Delta t_{n-1}$. This is a first order approximation to the stage value, whereas the others are of second order. However, it is closer to $t_n + c_1\Delta t_n$, which might make up for that. We thus tried both and found the methods to be almost identical. From this on we will use (15). Regarding quadratic extrapolation, it is reasonable to choose t_n, t_{n-1} and the intermediate temperature vector Θ_{n-1}^1 from the previous stage $t_{n-1} + c_1\Delta t_{n-1}$. This results in

$$\begin{aligned}\Theta_n^1 \approx \Theta_{n-1}\frac{(c_1\Delta t_n+(1-c_1)\Delta t_{n-1})c_1\Delta t_n}{c_1\Delta t_{n-1}^2} - \Theta_{n-1}^1\frac{(c_1\Delta t_n+\Delta t_{n-1})c_1\Delta t_n}{c_1\Delta t_{n-1}^2(1-c_1)} \\ +\Theta_n\frac{(c_1\Delta t_n+\Delta t_{n-1})(c_1\Delta t_n+(1-c_1)\Delta t_{n-1})}{(1-c_1)\Delta t_{n-1}^2}. \quad (16)\end{aligned}$$

At the second stage, we linearly extrapolate Θ_n at t_n and Θ_n^1 at $t_n + c_1\Delta t$ to obtain

$$\Theta_{n+1} \approx \Theta_n + \Delta t_n(\Theta_n^1 - \Theta_n)/(c_1\Delta t_n) = \left(1 - \frac{1}{c_1}\right)\Theta_n + \frac{1}{c_1}\Theta_n^1. \quad (17)$$

When applying quadratic extrapolation at the second stage (or at later stages in a scheme with more than two), it is better to use values from the current time interval. This results in

$$\begin{aligned}\Theta_{n+1} \approx \Theta_{n-1}\frac{\Delta t_n^2(1-c_1)}{\Delta t_{n-1}(\Delta t_{n-1}+c_1\Delta t_n)} - \Theta_n\frac{(\Delta t_{n-1}+\Delta t_n)(1-c_1)\Delta t_n}{\Delta t_{n-1}c_1\Delta t_n} \\ +\Theta_n^1\frac{(\Delta t_{n-1}+\Delta t_n)\Delta t_n}{(c_1\Delta t_n+\Delta t_{n-1})c_1\Delta t_n}. \quad (18)\end{aligned}$$

4.3 Flow over a plate

As a first test case, the cooling of a flat plate resembling a simple work piece is considered. The work piece is initially at a much higher temperature than the fluid and then cooled by a constant air stream, see figure 1.

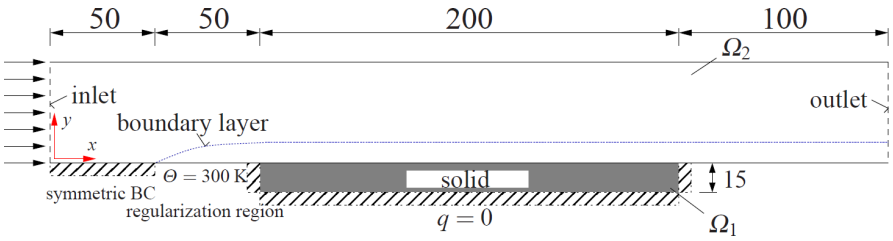

Fig. 1 Test case for the coupling method

The inlet is given on the left, where air enters the domain with an initial velocity of $\mathrm{Ma}_\infty = 0.8$ in horizontal direction and a temperature of 273 K. Then, there are two succeeding regularization regions of 50 mm to obtain an unperturbed boundary layer. In the first region, $0 \leq x \leq 50$, symmetry boundary conditions, $v_y = 0$, $q = 0$, are applied. In the second region, $50 \leq x \leq 100$, a constant wall temperature of 300 K is specified. Within this region the velocity boundary layer fully develops. The third part is the solid (work piece) of length 200 mm, which exchanges heat with the fluid, but is assumed insulated otherwise, thus $q_b = 0$. Therefore, Neumann boundary conditions are applied throughout. Finally, the fluid domain is closed by a second regularization region of 100 mm with symmetry boundary conditions and the outlet.

Regarding the initial conditions in the structure, a constant temperature of 900 K at $t = 0$ s is chosen throughout. To specify reasonable initial conditions within the fluid, a steady state solution of the fluid with a constant wall temperature $\Theta = 900$ K is computed.

The grid is chosen cartesian and equidistant in the structural part, where in the

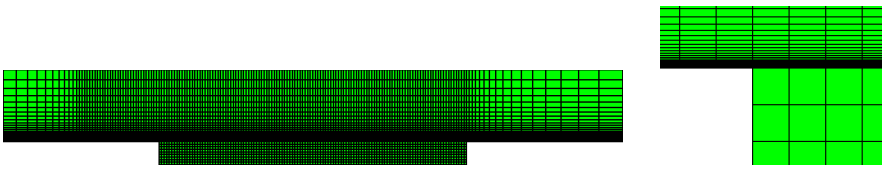

(a) Entire mesh (b) Mesh zoom

Fig. 2 Full grid (left) and zoom into coupling region (right)

fluid region the thinnest cells are on the boundary and then become coarser in y-direction (see figure 2). To avoid additional difficulties from interpolation, the points of the primary fluid grid, where the heat flux is located in the fluid solver, and the nodes of the structural grid are chosen to match on the interface Γ.

Table 1 Total number of iterations for 100 secs of real time without any extrapolation. Fixed time step sizes versus adaptive steering.

TOL	Fixed time step size		Time adapt., $\Delta t_0 = 0.5s$
10^{-2}	$\Delta t = 5s$	64	31
10^{-3}	$\Delta t = 5s$	82	39
10^{-4}	$\Delta t = 0.5s$	802	106

We now compare the different schemes for a whole simulation of 100 seconds real time. If not mentioned otherwise, the initial time step size is $\Delta t = 0.5s$. To first give an impression on the effect of the time adaptive method, we look at fixed time step versus adaptive computations in table 1. Thus, the different tolerances for the time adaptive case lead to different time step sizes and tolerances for the

nonlinear system over the course of the algorithm, whereas in the fixed time step size, they steer only how accurate the nonlinear systems are solved. For the fixed time step case, we chose $\Delta t = 0.5s$ and $\Delta t = 5s$, which roughly corresponds to an error of 10^{-2} and 10^{-3}, respectively 10^{-4}. Thus, computations in one line of table 1 correspond to similar errors. As can be seen, the time adaptive method is in the worst case a factor two faster and in the best case a factor of eight. Thus the time adaptive computation serves from now on as the base method for the construction of a fast solver.

Table 2 Total number of iterations for 100 secs of real time with extrapolation

TOL	none	lin.	quad.
10^{-2}	31	19	25
10^{-3}	39	31	32
10^{-4}	106	73	77
10^{-5}	857	415	414

Finally, we consider extrapolation based on the time integration scheme. In table 2, the total number of iterations for 100 seconds of real time is shown. As can be seen, linear extrapolation speeds up the computations between 20% and 50%. Quadratic extrapolation leads to a speedup between 15% and 50% being overall less efficient than the linear extrapolation procedure. Overall, we are thus able to simulate 100 seconds of real time for this problem for an engineering tolerance using only 19 calls to fluid and the structure solver each.

To understand this more precisely, we considered the second stage of the second time step in an adaptive computation. We thus have finished the first time step with $\Delta t_0 = 0.5s$ and the second time step gets doubled, leading to $\Delta t_1 = 1s$. This is depicted in Figure 3. To obtain a temperature for the new time t_{n+1} the linear extrapolation method (17) uses the values of the current time t_n and of the first Runge-Kutta Step at $t_1 + \Delta t_1 c_1$. As can be seen, this predicts the new time step very well. In contrast, the quadratic extrapolation (18) uses for the new time step the solution from the previous time t_0 the current time t_1 and from the first Runge Kutta stage. Since the exact solution has a more linear behavior in the time step, the quadratic extrapolation provides no advantage, in particular since it slopes upward after some point.

4.4 Cooling of a flanged shaft

As a second test case, we consider the cooling of a flanged shaft by cold high pressured air, a process that's also known as gas quenching. The complete process consists of the inductive heating of a steel rod, the forming of the hot rod into a flanged shaft, a transport to a cooling unit and the cooling process. Here, we consider only the cooling, meaning that we have a hot flanged shaft that is cooled by cold high

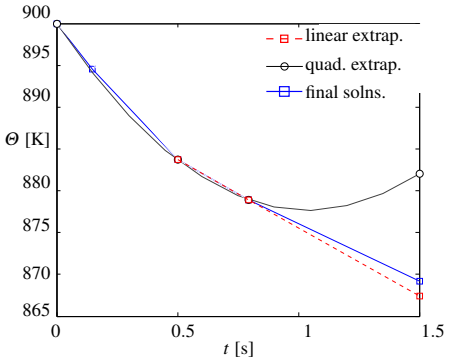

Fig. 3 Comparison of the linear and quadratic extrapolation methods for the time step $t = 1.5$s.

pressured air coming out of small tubes [25]. We consider a two dimensional cut through the domain and assume symmetry along the vertical axis, resulting in one half of the flanged shaft and two tubes blowing air at it, see figure 4. Since the air nozzles are evenly distributed around the flanged shaft, we use an axisymmetric model in the structure. The heat flux from the two-dimensional simulation of the fluid at the boundary of the flanged shaft is impressed axially symmetrical on the structure.

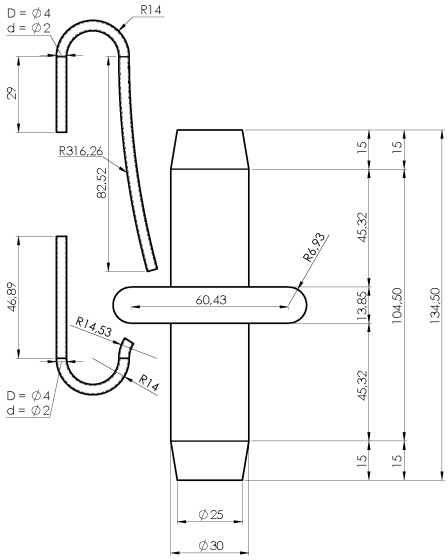

Fig. 4 Sketch of the flanged shaft

We assume that the air leaves the tube in a straight and uniform way at a Mach number of 1.2. Furthermore, we assume a freestream in x-direction of Mach 0.005. This is mainly to avoid numerical difficulties at Mach 0, but could model a draft in the workshop. The Reynolds number is $Re = 2500$ and the Prandtl number $Pr = 0.72$.

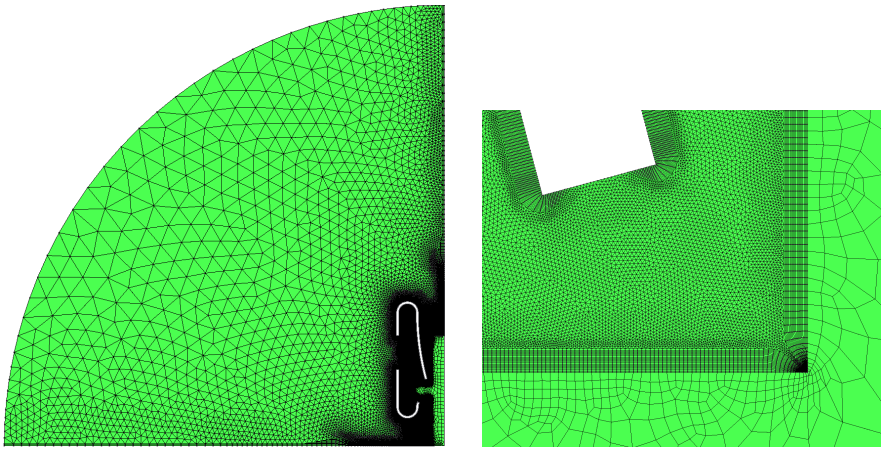

(a) Entire mesh (b) Mesh zoom

Fig. 5 Full grid (left) and zoom into shaft region (right)

The grid consists of 279212 cells in the fluid, which is the dual grid of an unstructured grid of quadrilaterals in the boundary layer and triangles in the rest of the domain, and 1997 quadrilateral elements in the structure. It is illustrated in figure 5.

To obtain initial conditions for the subsequent tests, we use the following procedure: We define a first set of initial conditions by setting the flow velocity to zero throughout and choose the structure temperatures at the boundary points to be equal to temperatures that have been measured by a thermographic camera. Then, setting the y-axis on the axis of revolution of the flange, we set the temperature at each horizontal slice to the temperature at the corresponding boundary point. Finally, to determine the actual initial conditions, we compute 10^{-5} seconds of real time using the coupling solver with a fixed time step size of $\Delta t = 10^{-6}s$. This means, that the high pressured air is coming out of the tubes and the first front has already hit the flanged shaft. This solution is illustrated in figure 6 (left).

Now, we compute 1 second of real time using the time adaptive algorithm with different tolerances and an initial time step size of $\Delta t = 10^{-6}s$. This small initial step size is necessary to prevent instabilities in the fluid solver. During the course of the computation, the time step size is increased until it is on the order of $\Delta t = 0.1s$, which demonstrates the advantages of the time adaptive algorithm and reaffirms that it is this algorithm that we need to compare to, see Fig. 7 left. In total, the time adaptive method needs 22, 41, 130 and 850 time steps to reach $t = 1s$ for the

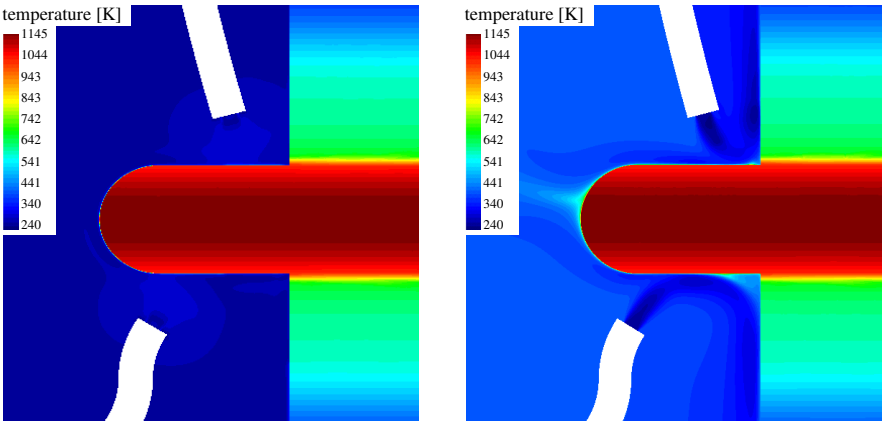

Fig. 6 Temperature distribution in fluid and structure at $t = 0s$ (left) and $t = 1s$ (right).

different tolerances, compared to the 10^6 steps the fixed time step method would need.

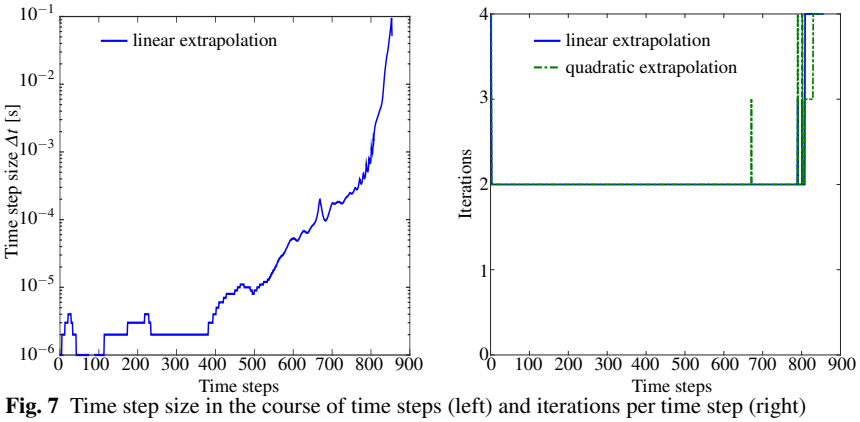

Fig. 7 Time step size in the course of time steps (left) and iterations per time step (right)

The solution at the final time is depicted in figure 6 (right). As can be seen, the stream of cold air is deflected by the shaft.

We now consider extrapolation based on the time integration scheme. In table 4, the total number of iterations for 1 second of real time is shown. As before, the extrapolation methods cause a noticable decrease in the total number of fixed point iterations. The linear and quadratic extrapolation, however, show a marked acceleration profit. For smaller tolerance measures $TOL \leq 10^{-4}$ the linear extrapolation method is slightly better than the quadratic one. For the tolerance $TOL = 10^{-5}$ a significant improvement of the quadratic extrapolation is shown. When looking at

the number of iterations per time step, it is only after about half of the time steps that quadratic extrapolation shows an advantage over the linear one. Then, the quadratic extrapolation method takes an average of only one iteration, while the linear method needs two iterations, see Fig. 7 right. Overall, the speedup from linear extrapolation is between 18% and 34%, compared to the results obtained without extrapolation. The speedup from quadratic extrapolation is between 10% and 35%.

Table 3 Total number of iterations for 1 sec of real time for different extrapolation methods in time.

TOL	none	lin.	quad.
10^{-2}	51	42	46
10^{-3}	126	97	96
10^{-4}	414	309	310
10^{-5}	2768	1805	1789

4.5 Heated rod

In a third example, we consider a rod, which is heated while suspended horizontally over a table in a wind tunnel. This corresponds to another basic experiment related to gas quenching of steel to study the coupling between the fluid and the solid. We assume a very long rod, so we choose a cut transverse to the rod and calculate this by a 2D simulation. The inflow is horizontally from the left with a velocity of 30 m/s, corresponging to $Ma_\infty = 0.0906$ and a temperature of 297K and at the lower side, we have no slip boundary conditions. In the middle of the rod is a heating element with a diameter of 10mm, which heats with 500W.

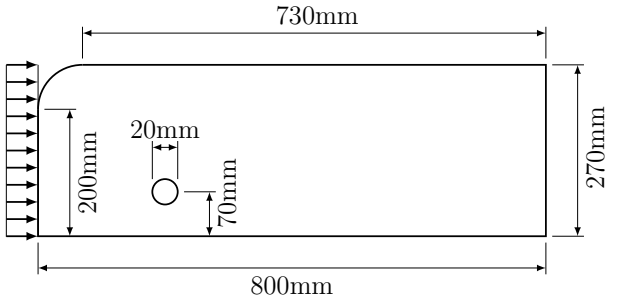

Fig. 8 Sketch of the heating rod

Both grids are unstructured with the fluid grid consisting of 236003 quadrilateral and triangular cells, see Fig. 9, whereas the solid grid has 1078 quadrilateral

elements. The Reynolds number for this test case is $Re = 406051$ and the Prandtl number is $Pr = 0.72$.

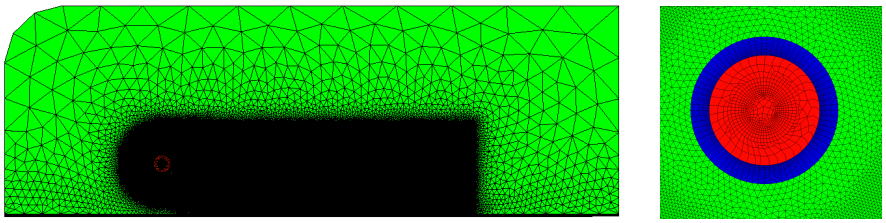

(a) Entire mesh (b) Mesh zoom

Fig. 9 Full grid (left) and zoom into rod region (right)

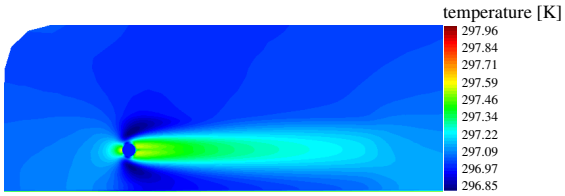

Fig. 10 Temperature distribution in fluid and structure at $t = 0s$ with entire domain.

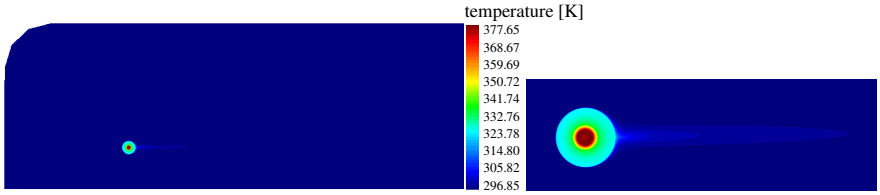

(a) Entire domain (b) Zoom

Fig. 11 Temperature distribution in fluid and structure at $t = 10s$ with entire domain (left) and snippet of the rod (right).

The initial condition for the solid is a constant temperature of 297K. The starting point of the fluid was conducted by a simulation until a steady state was established, see Fig. 10. As with the other examples, the adaptive time step control has a great advantage in the course of the computation. It starts with a time step size of $\Delta t = 10^{-6}$s and grows by the end of the simulation to $\Delta t = 4.19$s. The adaptive method needed for 10s of computation 59 - 299 time steps, a fixed time step size requires 10^7 steps. The solution at the final time $T = 10$s is depicted in figure 11. In the

outer regions a constant temperature can be seen, while behind of the rod due to the influence of the heating a thermal wake occurs.

In table 4, the total number of iterations for 10 second of real time is shown. For all tolerances the linear extrapolation method is slightly better than the quadratic one. In this case, none of the methods requires many iterations, so that none of the extrapolation methods has an advantage. Only with a decreasing tolerance limit $TOL \leq 10^{-4}$ for the subsolvers itself as well as for the coupling solver, the extrapolation procedures use their advantage. The speedup from linear extrapolation is between 11% and 16%, compared to the results obtained without extrapolation. The speedup from quadratic extrapolation is between 10% and 15%.

Table 4 Total number of iterations for 10 sec of real time for different extrapolation methods in time.

TOL	none	lin.	quad.
10^{-2}	59	57	59
10^{-3}	58	58	60
10^{-4}	99	88	89
10^{-5}	299	252	255

5 Summary and Conclusions

We considered a time dependent thermal fluid structure interaction problem where a nonlinear heat equation to model steel is coupled with the compressible Navier-Stokes equations. The coupling is performed in a Dirichlet-Neumann manner. As a fast base solver, a higher order time adaptive method is used for time integration. This method is significantly more efficient than a fixed time step method and is therefore the scheme to beat.

To reduce the number of fixed point iterations in a partitioned spirit, extrapolation based on the time integration was tried out. This reduces the number of iterations by up to 50%. Hereby, linear extrapolation works better than quadratic.

The combined time adaptive method with linear extrapolation thus allows to solve real life problems at engineering tolerances using only a couple dozen calls to the fluid and structure solver.

References

1. M. ARNOLD, *Stability of Sequential Modular Time Integration Methods for Coupled Multibody System Models*, J. Comput. Nonlinear Dynam., 5 (2010), pp. 1–9.
2. A. L. BANKA, *Practical Applications of CFD in heat processing*, Heat Treating Progress, (2005).

3. P. BIRKEN, *Termination criteria for inexact fixed point schemes*, Numer. Linear Algebra Appl., submitted.
4. P. BIRKEN, *Numerical Methods for the Unsteady Compressible Navier-Stokes Equations*, Habilitation Thesis, University of Kassel, 2012.
5. P. BIRKEN, K. J. QUINT, S. HARTMANN, AND A. MEISTER, *Chosing norms in adaptive FSI calculations*, PAMM, 10 (2010), pp. 555–556.
6. ———, *A Time-Adaptive Fluid-Structure Interaction Method for Thermal Coupling*, Comp. Vis. in Science, 13 (2011), pp. 331–340.
7. J. M. BUCHLIN, *Convective Heat Transfer and Infrared Thermography*, J. Appl. Fluid Mech., 3 (2010), pp. 55–62.
8. P. ERBTS AND A. DÜSTER, *Accelerated staggered coupling schemes for problems of thermoelasticity at finite strains*, Comp. & Math. with Appl., 64 (2012), pp. 2408–2430.
9. C. FARHAT, *CFD-based Nonlinear Computational Aeroelasticity*, in Encyclopedia of Computational Mechanics, E. Stein, R. de Borst, and T. J. R. Hughes, eds., vol. 3: Fluids, John Wiley & Sons, 2004, ch. 13, pp. 459–480.
10. T. GERHOLD, O. FRIEDRICH, J. EVANS, AND M. GALLE, *Calculation of Complex Three-Dimensional Configurations Employing the DLR-TAU-Code*, AIAA Paper, 97-0167 (1997).
11. M. B. GILES, *Stability Analysis of Numerical Interface Conditions in Fluid-Structure Thermal Analysis*, Int. J. Num. Meth. in Fluids, 25 (1997), pp. 421–436.
12. U. HECK, U. FRITSCHING, AND K. BAUCKHAGE, *Fluid flow and heat transfer in gas jet quenching of a cylinder*, International Journal of Numerical Methods for Heat & Fluid Flow, 11 (2001), pp. 36–49.
13. M. HINDERKS AND R. RADESPIEL, *Investigation of Hypersonic Gap Flow of a Reentry Nosecap with Consideration of Fluid Structure Interaction*, AIAA Paper, 06-1111 (2006).
14. U. KÜTTLER AND W. A. WALL, *Fixed-point fluidstructure interaction solvers with dynamic relaxation*, Comput. Mech., 43 (2008), pp. 61–72.
15. P. LE TALLEC AND J. MOURO, *Fluid structure interaction with large structural displacements*, Comp. Meth. Appl. Mech. Engrg., 190 (2001), pp. 3039–3067.
16. N. LIOR, *The cooling process in gas quenching*, J. Materials Processing Technology, 155-156 (2004), pp. 1881–1888.
17. R. C. MEHTA, *Numerical Computation of Heat Transfer on Reentry Capsules at Mach 5*, AIAA-Paper 2005-178, (2005).
18. C. MICHLER, E. H. VAN BRUMMELEN, AND R. DE BORST, *Error-amplification Analysis of Subiteration-Preconditioned GMRES for Fluid-Structure Interaction*, Comp. Meth. Appl. Mech. Eng., 195 (2006), pp. 2124–2148.
19. H. OLSSON AND G. SÖDERLIND, *Stage value predictors and efficient Newton iterations in implicit Runge-Kutta methods*, SIAM J. Sci. Comput., 20 (1998), pp. 185–202.
20. K. J. QUINT, S. HARTMANN, S. ROTHE, N. SABA, AND K. STEINHOFF, *Experimental validation of high-order time integration for non-linear heat transfer problems*, Comput. Mech., 48 (2011), pp. 81–96.
21. P. R. SPALART AND S. R. ALLMARAS, *A One-Equation Turbulence Model for Aerodynamic Flows*, AIAA 30th Aerospace Science Meeting, 92–0439 (1992).
22. P. STRATTON, I. SHEDLETSKY, AND M. LEE, *Gas Quenching with Helium*, Solid State Phenomena, 118 (2006), pp. 221–226.
23. S. VAN ZUIJLEN, A. H. BOSSCHER AND H. BIJL, *Two level algorithms for partitioned fluidstructure interaction computations*, Comp. methods appl. mech. eng., (2007).
24. J. VIERENDEELS, L. LANOYE, J. DEGROOTE, AND P. VERDONCK, *Implicit Coupling of Partitioned Fluid-Structure Interaction Problems with Reduced Order Models*, Comp. & Struct., 85 (2007), pp. 970–976.
25. U. WEIDIG, N. SABA, AND K. STEINHOFF, *Massivumformprodukte mit funktional gradierten Eigenschaften durch eine differenzielle thermo-mechanische Prozessführung*, WT-Online, (2007), pp. 745–752.
26. O. ZIENKIEWICZ AND R. TAYLOR, *The Finite Element Method*, Butterworth Heinemann, 2000.